



Microscopic insight into the bilateral formation of carbon spirals from a symmetric iron core

SUBJECT AREAS:

SYNTHESIS AND
PROCESSING

NANOWIRES

APPLIED PHYSICS

NANOPARTICLES

Hidetsugu Shiozawa¹, Alicija Bachmatiuk², Andreas Stangl¹, David C. Cox³, S. Ravi P. Silva³, Mark H. Rummeli^{2,4} & Thomas Pichler¹

¹Faculty of Physics, University of Vienna, Strudlhofgasse 4, 1090 Wien, Austria, ²IFW Dresden, P.O. Box 270116, D-01171 Dresden, Germany, ³Advanced Technology Institute, University of Surrey, Guildford, GU2 7XH, UK, ⁴Center for Integrated Nanostructure Physics, Institute for Basic Science, Department of Energy Science, Sungkyunkwan University, Republic of Korea.

Received
7 February 2013

Accepted
25 April 2013

Published
14 May 2013

Correspondence and
requests for materials
should be addressed to
H.S. (hidetsugu.
shiozawa@univie.ac.at)

Mirrored carbon-spirals have been produced from pressured ferrocene via the bilateral extrusion of the spiral pairs from an iron core. A parametric plot of the surface geometry displays the fractal growth of the conical helix made with the logarithmic spiral. Electron microscopy studies show the core is a crystalline cementite which grows and transforms its shape from spherical to biconical as it extrudes two spiralling carbon arms. In a cross section along the arms we observe graphitic flakes arranged in a herringbone structure, normal to which defects propagate. Local-wave-pattern analysis reveals nanoscale defect patterns of two-fold symmetry around the core. The data suggest that the bilateral growth originates from a globular cementite crystal with molten surfaces and the nano-defects shape emerging hexagonal carbon into a fractal structure. Understanding and knowledge obtained provide a basis for the controlled production of advanced carbon materials with designed geometries.

The discovery of new forms of inorganic nanomaterials with advanced properties has opened exciting possibilities in nanosciences. A large variety of nanomaterials were synthesised via methods from colloidal synthesis of quantum dots and metal clusters¹ to physical synthesis of molecular nanostructures^{2–4}. The unique physical and chemical properties of nanomaterials stem from their nanoscale structures which allow quantum effects to emerge. The synthesis of predefined structural dimensions and geometries is of great importance and hence, understanding and control of nanoscale shape formation are major focuses in materials science. On one hand, complex inorganic nanostructures such as polyhedral metals⁵, helical oxides^{6,7} and semiconductors⁸, and helical carbon nanotubes⁹ can be formed as a result of crystallographic and defect arrangements. On the other hand, the size and shape of nuclei, seeds or catalysts play important roles in promoting chemical processes in the production of low dimensional nanostructures, such as semiconducting nanowires¹⁰, carbon nanotubes (CNTs)³ and graphene⁴. When nanowires or nanotubes grow via the vapour-liquid-solid mechanism¹¹, catalyst nanoparticles nucleate and extrude a 1D structure from one side of the particle¹². The epitaxial growth of graphene via the chemical vapour deposition (CVD) method generally requires an atomically flat metal surface to catalyse and support the self-organisation of carbon atoms in a hexagonal form with one atom thick. As such, the way atoms and molecules are assembled into nanostructures depends critically on the shape of the catalysts prepared in advance or formed in the course of the synthesis¹³.

In this paper, we study the formation mechanism for bilateral carbon spirals, with special emphasis on the role of metal catalysts and defects. The spiral samples are grown by the pyrolysis of pure ferrocene vapour at high pressure in a sealed volume¹⁴. At effective ferrocene pressures greater than 5 MPa, the catalytic activity on the created metal particle is polarized bilaterally so that it forms a pair of carbon arms out of an almost spherical metal surface. This stands in stark contrast to the cases for CNTs and graphene where *sp*² carbon layers grow unilaterally from one side of the catalyst only.

The novelty of this bilateral carbon formation is manifested by the unique morphology that is transposed on the fully symmetric structures from nanoscale to microscale. Scanning electron microscopy (SEM) observations show that the symmetric objects are produced in large yield and high purity (see the SEM micrograph provided in the supplementary material). Most of the objects observed exhibit a similar morphological identity whilst there are variations in size and shape. The fact that the arms are conical and each arm is a mirrored shape of the other, can be explained by our growth model¹⁴; two carbon arms are extruded bilaterally from the opposite side of the



symmetric core, resulting in its mirrored shape. The cone shape of the arms occurs as a result of the core growing simultaneously as the arms grow out of the core. A fascinating feature of this novel nanostructure is its spiralling arms. Its high reflectional symmetry ensures that the helicity of one arm is mirrored to the other in an opposite orientation. Although some of the key features of the mirrored objects were highlighted in our previous paper¹⁴, microscopic details of the bilateral growth is yet to be explained and the growth mechanism elucidated for the complex spiralling shapes. Knowing microscopic details of the interior structures of the micro objects will allow us to understand the cause of the symmetric growth, hence provide a deeper insight into the origin of the emergence of complex shape symmetry that spontaneously occurs at the nanoscale.

We show from SEM observations of different samples that the iron core transforms its shape from a original sphere to a bicone as the carbon arms end spiralling. The spiralling morphologies are reproduced by a parametric plot that exhibits the fractal growth of the bilateral conical helix made with the logarithmic spirals. Microscopic insight into the symmetric growth is sought via cross-sectional transmission electron microscopy (TEM) studies of spiral samples. Selected area electron diffraction (SAED) patterns acquired across the cross-section of a spiral show graphite [002] diffractions whose orientations are found to be consistent with the reflectional symmetry of the surface morphology and constitute herringbone structures within the arm's cross section. Nanometer-scale patterns of defects are observed by TEM in the same cross-section. Long-range properties of the defect patterns are exploited via mapping of the local wave orientation^{15,16}. The image obtained exhibits two-fold symmetry around the core, ascertaining the herringbone arrangement of nano-defects roughly normal to the layer of graphite flakes. This provides us an important insight that the defects propagate normal to the graphite layers as the arms grow. Such defect arrangements could be created as a result of temporal anomalies or instabilities in growth reaction on the core surface which must be molten at a high temperature. The defects are then arranged at the nanoscale to form complex shapes of micro-objects from hexagonal carbon.

Insights we gained for the bilateral and spirals' formation could have fundamental and practical implications for understanding and control of a variety of complex microscopic forms as well as for defect engineering for graphene and carbon nanotubes¹⁷. Hence, the present work provide alternative experimental and methodological pathways to a better understanding of pattern formation in nature.

Results

Bilateral and spiralling morphology. Fig. 1 shows the SEM micrographs of carbon-spirals which show evolutionary changes in shape. In the micrographs it is clearly observed that larger samples have a more rectangular core and smaller samples have a more spherical core. The longer the objects, the straighter the arms while the smaller arms have more twisted spiralling sections. They are different in size, but all share a unique geometrical character with reflectional symmetry. The arms are observed to be almost isotropic or circular in cross sections normal to the arms axis, attaining a 3D conical structure. The iron core is observed as a bright area at the center of the sample. The shape and diameter of the core depend on the sample dimension. In the larger samples the core is more rectangular in contrast to the more rounded shapes found in the smaller samples that only have spiralling arms. According to the model proposed previously¹⁴, the arms are formed symmetrically from opposite sides of the catalyst core. In this case, the cone shape of the arms is explained as a result of the growing iron core from which the carbon arms are extruded in opposite directions. This implies that the iron and carbon elements must be supplied through a mirror plane. The arms spiral only when the core is small, hence the

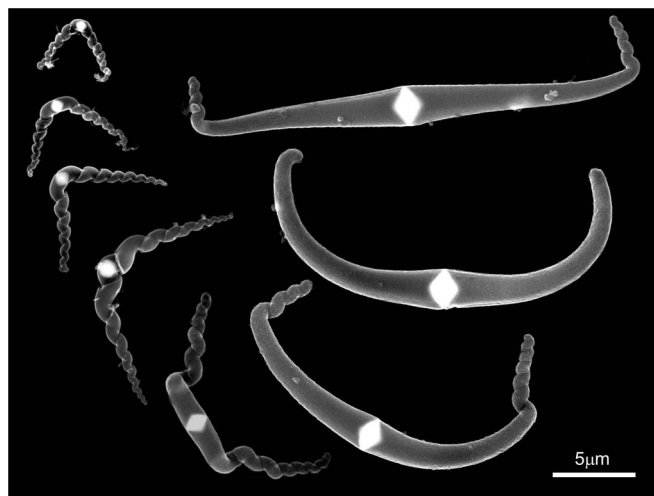


Figure 1 | SEM micrographs of bicone spirals of different sizes.

arms of the smaller samples are more twisted. The opposite helicity of the spirals between the left and right arms supports the bilateral growth model.

Parametric plot. According to the mathematical prediction suggested in the previous work¹⁴, the length of the cone extrapolated to the imaginary cone apex L is linearly related to the radius of the spherical core R , with the cone angle ~ 0.15 radians ($\sim 8.6^\circ$). This model was successful in explaining the experimental results. Here, the method of hodograph is adapted to produce spiralling extrusions of carbon arms from a catalyst core, in analogy to the mechanism suggested for helical carbon nanotube growth⁹. We introduce a linear gradient of the growth rate $\Delta\theta$ across the cones' base that revolves around the core with an angular velocity $\Delta\phi$ [rad.]. This creates helical arms whose surface can be drawn by arrays of circles distanced by ΔT_i [μm] ($i = 0, 1, 2, \dots$) which increase over time and titled against one another by $\Delta\theta$ [rad] towards the polar angle rotated by $\Delta\phi$ [rad.], see the schematic diagram in Fig. 2. The tip radius and the cone angle are given by the initial radius r_0 [μm] and its increment Δr_i [μm], respectively. With fitted parameters; $\Delta T_i = 0.15i$ [μm], $\Delta\theta = 0.16$ rad. ($\sim 9.0^\circ$), $\Delta\phi = 0.21$ rad. ($\sim 12.0^\circ$), $r_0 = 0.22$ μm and $\Delta r_i = 0.01i$ [μm], the recursive helical arrangement of the cone units reproduces well the morphology of spiralling arms, shown as upper three sequential images for growing mirrored cone spirals in Fig. 2. This result provides two important insights into the spiral geometry. Firstly, the linearly increasing ΔT_i and Δr_i with the other parameters constant lets the locus of the spiralling cone create a conical spring with its tangential linear hyperbola, and hence each i component of the spiral is self-similar to one another which is a property of fractal growth. Its projection to a plane normal to the growth direction should then be the logarithmic spiral. Secondly, the two spiralling arms are connected to each other at the cone base, that makes them angled against each other with the angle intrinsic to the spiral geometry.

In turn, the larger objects have straighter arms with kinked spiralling tips, i.e. the largest object seen in Fig. 1. Such can be produced under the condition that the spiralling stops at a point in time (at a cone length of T_ϕ), then the rate gradient goes to zero at a later time (at a cone length of T_θ). Fig. 2 shows simulated sequential images for a growing cone pair of a greater size. By using the offset functions $\Delta\phi \times [1 - u(T - T_\phi)]$ ($T_\phi = 4.6$ μm) and $\Delta\theta \times [1 - u(T - T_\theta)]$ ($T_\theta = 5.6$ μm) as inserted in the figure, the geometrical figure of the final product represents the appearance of the objects observed in the SEM micrographs. The movie for growing spiral pairs is provided as supplementary material. Here, good agreement between the

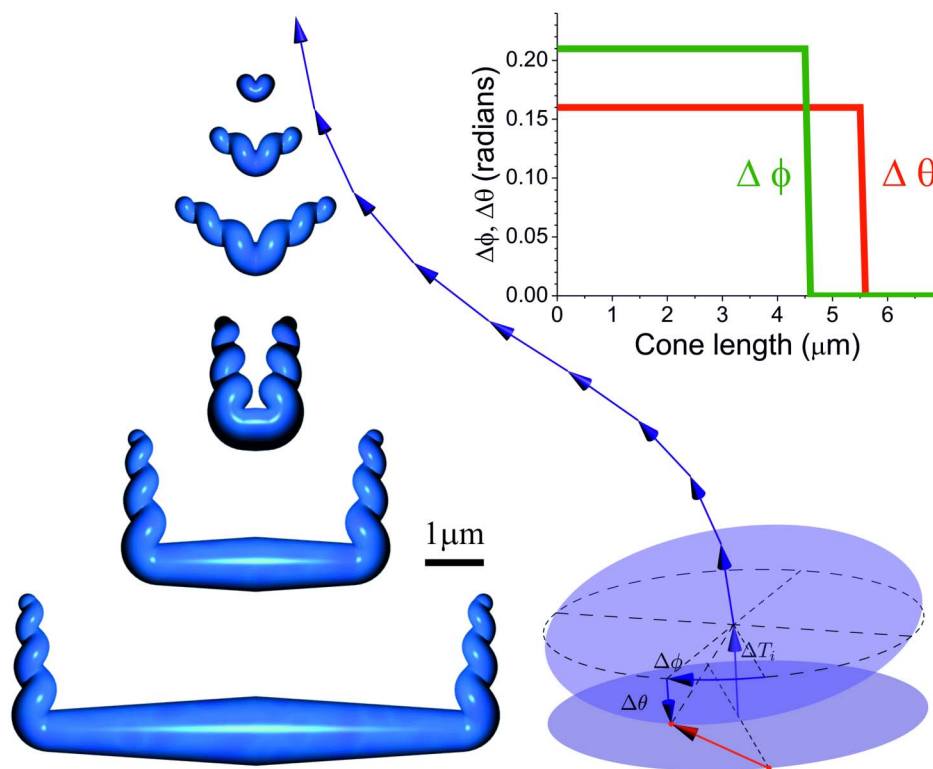


Figure 2 | Spiralling and kinked bicones produced by a hodographic method using parameters ($\Delta\phi$, $\Delta\theta$, and ΔT_i) as a function of the cone length.

simulation and experimental observations validates the proposed growth mechanism including the revolving gradient of the growth rate as the cause of mirrored spirals.

Size and shape of the core. The core morphology of the catalyst, which varies over time, plays an important role in the formation and structure of the arms extruded from the iron core. Here, the size and shape of the core are analyzed extensively for samples of different sizes. In the analysis we fit the cross sectional shape of the core with a rectangle (with the height a and width b) whose edges are truncated by a circle with radius r_e . This geometrical shape fits well with the

observed core shapes. In three dimensions, a and b represent the base radius and the height of the bicones, respectively, see the diagrams in Fig. 3. We define the shape factor, $f = r_e/a$. $f = 0$ means the core is an absolute rectangle in cross section (bicones in 3D). With increasing f the core becomes more rounded and eventually becomes circular in cross section (spherical in 3D) at $f = 1$.

In Fig. 3, the shape factor and cone angle α , derived as $\alpha = 2 \tan^{-1}(a/b)$, are plotted against the cone radius in μm . α stays nearly constant at $\sim 105^\circ$ over radii down to $0.5 \mu\text{m}$ at which point it starts to decline to as small as $\alpha \sim 85^\circ$ as the radius decreases. This indicates the iron bicones get flatter with increasing the cone radius, but this

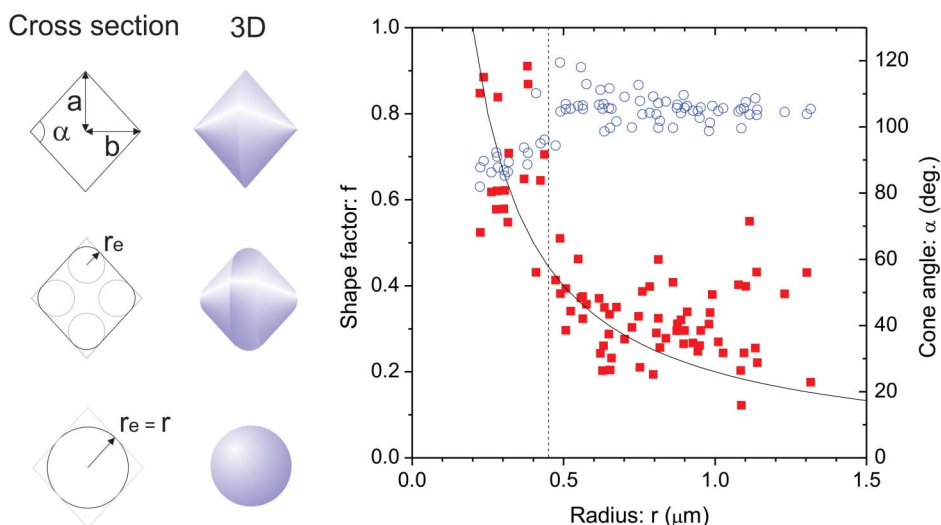


Figure 3 | Shape factor ($f = r_e/a$) and cone angle ($\alpha = 2 \tan^{-1}(a/b)$) of the iron core plotted against the core radius. Schematics on the left are truncated rectangular cores in cross section (2D) and corresponding bicones (3D).



change is minor, only within 20% of the absolute value. A more appreciable dependency of the shape factor on the cone radius is seen for the shape factor that, within the experimental error, decreases from $f \sim 0.9$ down to ~ 0.2 when the cone radius increases from $a \sim 0.2$ to $\sim 1.0 \mu\text{m}$.

The edge radius is found to be $r_e \sim 0.2 \mu\text{m}$ for all samples. This suggests that the rapid decrease of the shape factor is induced as a result of each hemisphere of the initially globular core ($r \sim 0.2 \mu\text{m}$) growing linearly in diameter towards the hemisphere base so that the core shape transforms from a sphere to a bicone whilst the curvature of the cone apex keeps the original hemisphere shape. Indeed, the shape factor follows the curve $0.2r^{-1}$, as plotted in Fig. 3. This fact could indicate that when the core grows, iron and carbon atoms diffuse into the bulk of the core rather than the interface between the core and carbon arms. In the latter case, the elements are added into the interface and their deposition on the sphere would modify the apex curvature significantly.

Experimentally, the changes both in shape factor and cone angle seem to profound when the core radius reaches around $0.45 \mu\text{m}$, as indicated by the vertical line in Fig. 3. This line separates the two regions in radius. In the small-radius region ($a < 0.45 \mu\text{m}$), the cores are almost circular in cross-sectional shape with the arms growing in twists. In the large-radius region ($a > 0.45 \mu\text{m}$), the cores become more rectangular in cross section with the arms growing straighter. This core-shape transition from the sphere to the bicones ends the twisting growth of the paired carbon arms. This provides us key information for understanding how the iron core templates the formation of spiralling carbon arms and how this could be correlated with the structural morphologies at atomic scales, as discussed in the following.

Crystal structure of the core. We now look into the atomistic detail of the core. Fig. 4 shows SAED patterns obtained at the positions across the core region. The almost identical patterns across the core are fitted well with the [122] diffraction of cementite Fe_3C [space group: $Pnma(62)$, $a = 5.0825 \text{ \AA}$, $b = 6.733 \text{ \AA}$, $c = 4.5119 \text{ \AA}$], suggesting that the core is a crystalline cementite of micrometer

across. The graphite layers grow out of the four cuts of the micro cementite core, whose Miller index can be identified exactly as the (2-1 0) facet for the upper right (lower left) area and the (2 3-4) facet for the upper left (lower right) area. Considering that the core surface is not necessarily normal to the observed cross section, the closest lower index facets are (1 0 0) and (2 0-1), respectively. From SAED observations on similar samples the lowest Miller index surface is found to match one of the core surface at least, indicating importance of the crystallographic arrangements on the emergence of the bilateral symmetry.

From the SEM study on various samples we have found that the core is made of truncated paired cones. Its rotational symmetry around the arm's axis means that the determined facets can't coincide with every hyperbola of the cones. Yet, it is possible to approximate the paired cone, for instance, by a n -fold dipyrmaid that has n equivalent facets around the arm's axis, on which the graphite layers grow. Such bilateral crystals can be formed based on the $Pnma$ structure, e.g. Ref. 18. Alternatively, the induction of defects can lead to a bilateral symmetry such as those found in decahedral gold⁵. The fact is that the bilateral growth of carbon arms originates at a point in time when the core is globular. The bilateral symmetry of the crystalline core allows pairs of low index facets at opposite ends to have a lower activation energy for graphite growth (higher-index facets of metal generally exhibit higher catalytic activity¹⁹), leading to a spontaneous emergence of the bilateral carbon nanostructure. Such symmetry breaking is known to occur in the growth of fcc metal nanocrystals of high aspect ratio where crystal symmetry is lowered from a more isotropic seed crystal to the formation of noble metal (Au, Ag, Pd) rods²⁰, and Pt multipods²¹ whose morphology defined by the number of twin defects. In our case, the symmetry breaking led to the extrusion of two graphite arms from a crystalline metal core rather than the deformation of the metal itself. This argument is similar to a bilateral carbon wire growth from a crystalline Co_3O_4 cluster²².

As the arms grow further, the core transforms its surface geometry into a pair of cones. From the SEM observations of the spirals of different sizes, we know that the edge radius is $\sim 0.2 \mu\text{m}$, invariant of

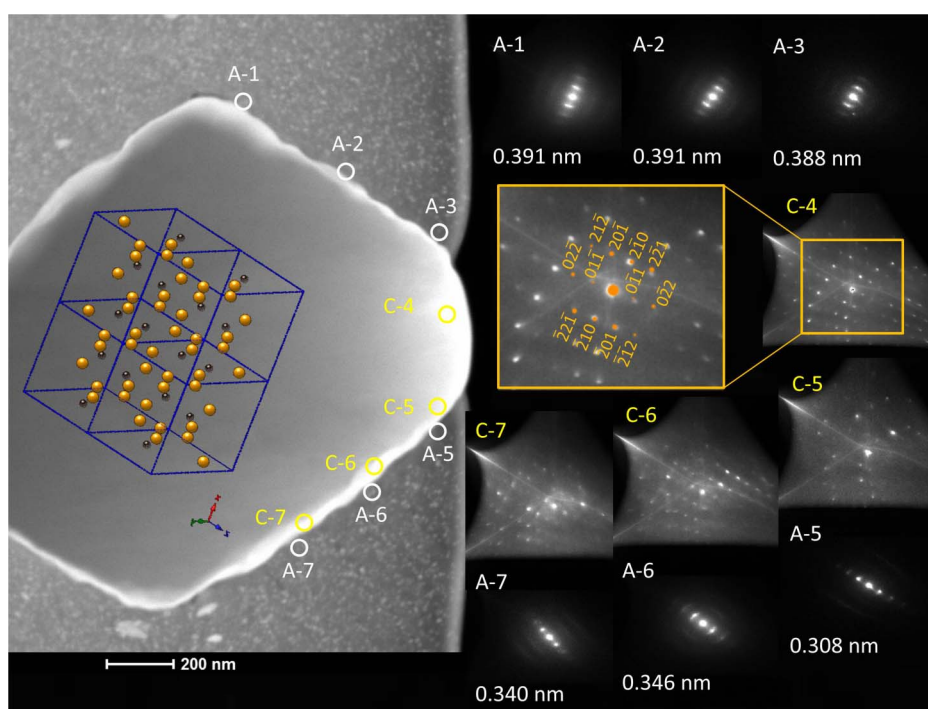


Figure 4 | SAED patterns collected on the core (C-5 to C-7) and on the arm (A-1 to A-7). The SAED patterns collected across the core show almost identical patterns which can be assigned to the [122] diffraction of cementite Fe_3C [space group: $Pnma(62)$, $a = 5.0825 \text{ \AA}$, $b = 6.733 \text{ \AA}$, $c = 4.5119 \text{ \AA}$].



the core radius, as ascertained by the $0.2 r^{-1}$ dependency of the shape factor in Fig. 3. This could indicate that the twin cones are formed by the enlargement of low-surface-energy facets of the cones via diffusion and deposition of iron carbide molecules into the bulk of the core, according to the Wulff construction.

Internal structure of the arm. Now, the question is how the arm's helical symmetry is created from a crystal core via the extrusion of graphenes which have D_{6h} structural symmetry. In the left panel of Fig. 5 is a TEM micrograph of a cross sectional cut of a carbon spiral, accompanied by SAED patterns (inserts) obtained at the positions marked by the open circles 1–8 in the TEM micrograph. All show predominantly the [002] diffraction of graphite. The interlayer spacings estimated from the diffraction patterns are 0.365 ± 0.024 nm. A distinctive feature observed across the arm is that the orientations of graphite in the left area (1, 2, 3 and 4) and right area (5, 6, 7 and 8) of the arm are almost each other's mirror image along the curving axis of the arm. The average difference in orientation of the graphite c -axis between the left and right is 83.5° .

The right panel in Fig. 5 is the magnified TEM micrograph of the same cross sectional cut provided in the left panel. The dark rectangular object is the iron core. Within the arms, patterns of dark and bright contrast bands are observed. It shows a herringbone-like pattern that resembles the appearance of leaf's veins, in which the angle of the fish bones leans upwards in the upper arm (the fish heading downwards), opposite to the orientation of the graphite layers observed with SAED (the fish heading upwards). Additionally, there is a bright spot observed in the vicinity of the tip of the iron cone, originating from which are some linear bright contrasts extending parallel to the arm's axis, resembling a fish spine. High-resolution TEM observations show the bright contrasts originate from defects in the graphite (see supplementary material), hence the herringbone pattern observed is a pattern formed by defects in the cross sectional plane of the graphite arm.

Defect patterns and local wave orientation analysis. In order to identify this defect pattern's geometry on a large scale, we process the

TEM data according to methods used for calculating local pattern properties of randomly oriented ripples, wrinkles or stripes such as those seen in Rayleigh-Bénard convection¹⁵. Assuming that the defect patterns are local stripes whose orientation varies on a longer spatial scale, we can approximate the local defect patterns for a given spatial coordinate (i, j) in the TEM micrograph by a two-dimensional wave: $u_{ij}(\vec{x}) = A_{ij} e^{i \vec{k}_{ij} \cdot \vec{x}}$, where \vec{k}_{ij} is the wave vector, \vec{x} the vector coordinate originating from the position (i, j) and A_{ij} is the amplitude.

In practice, we set a rectangular area ($|x| \leq 0.042 \mu\text{m}$ and $|y| \leq 0.014 \mu\text{m}$) along an azimuthal angle Θ_A centered at a spatial coordinate (i, j) in the TEM micrograph, and obtain the integrated intensity profile $u_{ij}(x)$ as the superposition of fields of all possible k . We perform Fast Fourier Transform (FFT) to get $u_{ij}(k) = \mathcal{F}_x[u_{ij}(x)](k)$ for n different Θ_A from 0 to $\pi - (1/n)\pi$. The *local wave orientation* Θ_{LW} and *wave length* λ_{LW} for a given (i, j) are then defined by the Θ_A and k for the greatest $u_{ij}(k)$. They are determined for all coordinates (i, j) across the spiral sample in the TEM micrograph, and then we obtain a coloured map of Θ_{LW} as depicted in Fig. 6. The image obtained provides an overview of the defect pattern geometry across the cross-sectional sample.

In the top arm we see a colour contrast between the left and right area. The left area is dominated by green and cyan, in contrast to the right area in which more blue and violet are observed. Conversely, the bottom arm exhibits a colour contrast reversed left and right. Green and cyan correspond to $\Theta_{LW} \sim 54 \pm 12^\circ$ from the horizontal axis and blue and violet $\Theta_{LW} \sim 138 \pm 12^\circ$. These two mean angles ($\Delta\Theta_{LW} \sim 84^\circ$) are nearly orthogonal to the c -axis of graphene obtained from the SAED data in Fig. 5, which means that the defects propagate normal to the graphite layer. This suggests that all atomic-scale imperfections and defects of the already-made graphite flakes or their boundaries are not the preferred site on which new flakes grow. In this case, the defect-nucleation coordinate on the core surface has to be displaced from its original position, otherwise the defects should propagate parallel to the arm's growth axis if the defects were created at a fixed coordinate on the core surface. In

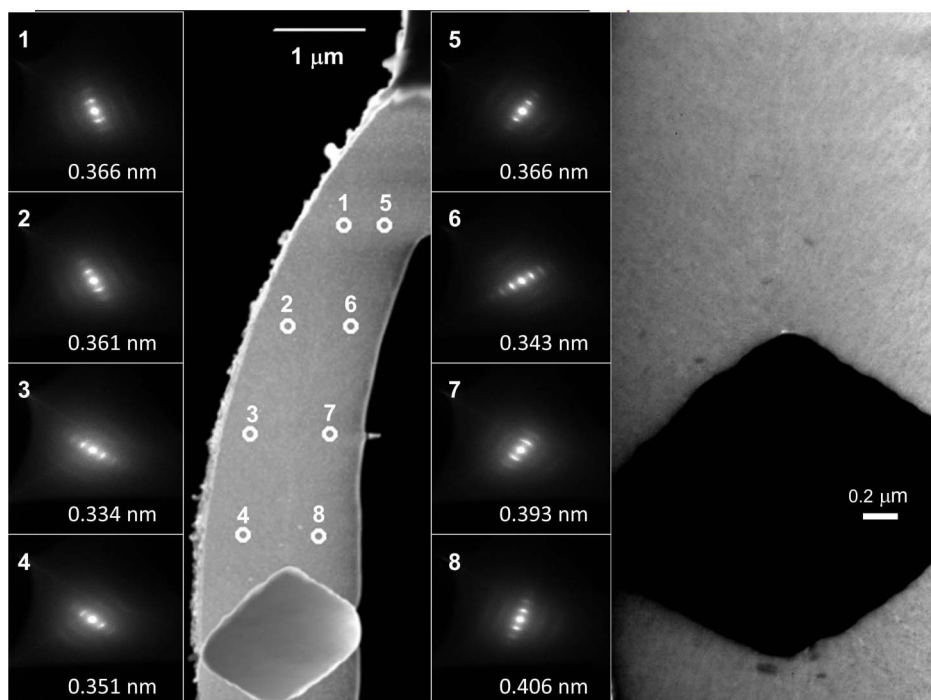


Figure 5 | Left: SAED patterns (1–8) collected across the arm's cross section showing graphite [002] diffractions. Right: high-resolution TEM around the iron core.

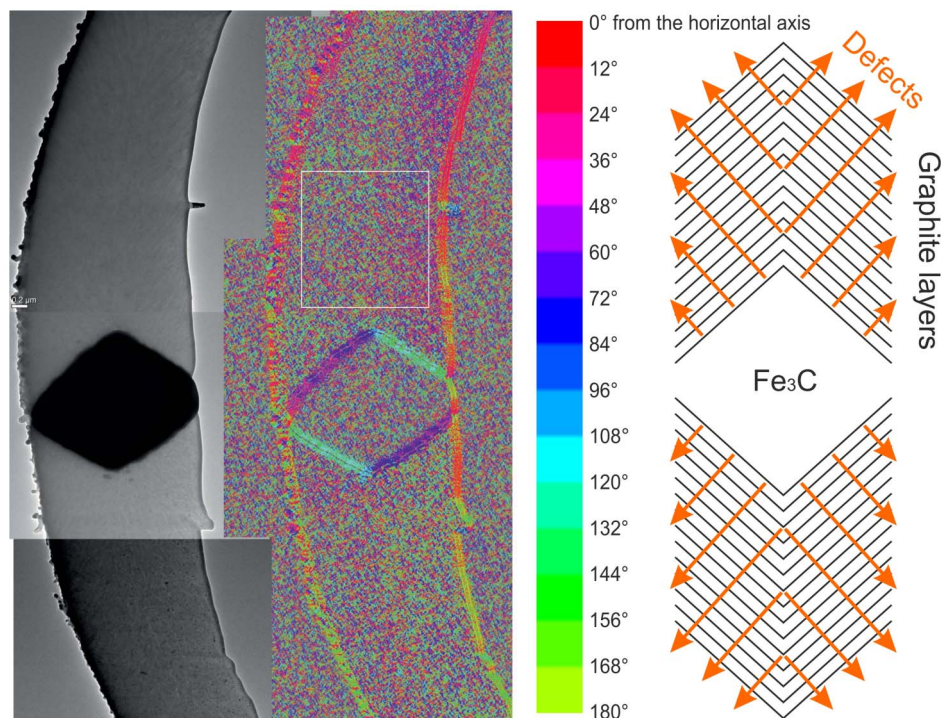


Figure 6 | Left: TEM micrograph and local wave orientation Θ_{LW} map of a cross sectional specimen of a bicone. Right: Schematics for a cross section of graphite arms in which defects propagate normal to graphite layers.

other words, the defects must be created as a result of temporal fluctuations in growth reaction on a molten core surface.

The local wave length λ_{LW} defines the mean spatial distance between the parallel line defects present in the carbon arm. The average of the local wavelengths across the rectangular area in Fig. 6b is 43 ± 16 nm, which is smaller by two-to-three orders than the scale of the arm's spiralling structures around 1–10 μ m. This fact leads us to an important conclusion that the micro curvature of the spiralling arms is not a direct consequence of atomic arrangements, as in the case of fullerenes or spiralling carbon nanotubes where pentagonal arrangements of carbon induce curvatures in hexagonal carbon nanostructure, but is produced via the induction of nanostructured defects.

Discussion

For the origin of the spiral formation to be understood, it is valuable to refer to studies on inorganic helical nanostructures. A variety of spiralling nano-objects produced so far include helical carbon fibres²³, helical nanotubes⁹, Si₃N₄²⁴, SiO₂ nanosprings⁶, ZnO nanohelices⁷ and PdS helical branched nanowires⁸. Inorganic helical nanostructures were suggested to be formed via epitaxial growth in which a screw dislocation along the growth axis allows helical structures to emerge²⁵. Carbon nanotubes can theoretically be coiled by the inclusion of pentagons and heptagons into the hexagonal lattice²⁶. Carbon coils reportedly require added catalysts or sulfuric impurities²⁷ to be produced by CVD. Interestingly, some of the resulting carbon coils seem to be formed bilaterally from a catalyst particle, that resembles our spiralling bicone despite differences in size and shape symmetry. To the best of our knowledge, no such bilateral growths were observed for straight CNTs, which indicates a possible correlation between spiralling and bilateral growth. A key to this problem would be the coherence of the reaction process. It is noted that a temporal coherence in growth reaction is a prerequisite for the helical structures to be formed. Such a condition could be provided as the periodic instability suggested for undulating Si nanowire growth in which the undulation of the diameter occurred only

for thinner Si wires¹⁰. This is in line with our observations on the spiralling as a function of the arm's radius and indicates a universal trend that such periodic instabilities emerge to appear only when the system considered is suitably compact.

In summary, using the state-of-the-art electron microscopy we have gained atomistic insight into the bilateral formation of symmetric carbon spirals. We found that the catalyst core is a crystalline cementite and the carbon arms are composed of graphitic flakes arranged in a herringbone structure, as hyperbolas of stacked cones in three dimensions. Local-wave-vector analysis with combined high-resolution TEM observations shows the defects propagate normal to the graphite planes. These observations show that the coherent defect arrangements at the nanoscale allow hexagonal carbon to be arranged for the fractal growth of the bilateral conical helix made with the logarithmic spirals. Further microscopy studies would shed light on the helical growth, especially in the arm's spiralling section where nanodefects could be arranged to have helical symmetry. The knowledge obtained throughout this study helps us understand the self organisation of carbon into complex structures, and hence provides a basis for the design of new carbon materials.

Methods

Ferrocene (~ 35 mg) was vacuum-sealed in a borosilicate glass ampoule (outer diameter = 6 mm, inner diameter = 3 mm, length ~ 33 mm) and then placed in a tube furnace at 625 °C for one hour, followed by cooling down to room temperature.

Scanning electron microscopy (SEM) images were obtained using a FEI Quanta 200F ESEM. Transmission electron microscopy (TEM) was conducted using a FEI Titan (80–300 kV, Monochromator-FEG, Cs-Corrector). The TEM specimens of about half micrometer thick were prepared using a FEI Nova Nanolab 600 Dual Beam Microscope that combines a high-resolution field emission SEM with a focused ion beam (FIB) for etching and deposition. The micro-cones are first covered in the FIB with ~1 μ m of tungsten deposit and are ion milled at 500 pA for the initial thinning and then thinned further and finally polished at 30 pA.

1. Murray, C. B., Kagan, C. R. & Bawendi, M. G. Synthesis and characterization of monodisperse nanocrystals and close-packed nanocrystal assemblies. *Annual Review of Materials Science* **30**, 545–610 (2000).
2. Kroto, H. W., Heath, J. R., O'Brien, S. C., Curl, R. F. & Smalley, R. E. C60: Buckminsterfullerene. *Nature* **318**, 162–163 (1985).



3. Iijima, S. Helical microtubules of graphitic carbon. *Nature* **354**, 56–58 (1991).
4. Novoselov, K. S. *et al.* Electric field effect in atomically thin carbon films. *Science* **306**, 666–669 (2004).
5. Johnson, C. L. *et al.* Effects of elastic anisotropy on strain distributions in decahedral gold nanoparticles. *Nature Materials* **7**, 120–124 (2008).
6. Zhang, H., Wang, C., Buck, E. & Wang, L. Synthesis, characterization, and manipulation of helical SiO₂ nanosprings. *Nano Lett.* **3**, 577–580 (2003).
7. Gao, P. X. *et al.* Conversion of zinc oxide nanobelts into superlattice-structured nanohelices. *Science* **309**, 1700–1704 (2005).
8. Bierman, M. J., Lau, Y. K. A., Kvit, A. V., Schmitt, A. L. & Jin, S. Dislocation-driven nanowire growth and eshelby twist. *Science* **320**, 1060–1063 (2008).
9. Amelinckx, S. *et al.* A formation mechanism for catalytically grown helix-shaped graphite nanotubes. *Science* **265**, 635–639 (1994).
10. Givargizov, E. I. Fundamental aspects of vls growth. *Journal of Crystal Growth* **31**, 20–30 (1975).
11. Wagner, R. S. & Ellis, W. C. Vapor-liquid-solid mechanism of single crystal growth. *Appl. Phys. Lett.* **4**, 89–90 (1964).
12. Shiozawa, H. *et al.* A catalytic reaction inside a single-walled carbon nanotube. *Adv. Mater.* **20**, 1443–1449 (2008).
13. Shiozawa, H. *et al.* Catalyst and chirality dependent growth of carbon nanotubes determined through nano-test tube chemistry. *Adv. Mater.* **22**, 3685–3689 (2010).
14. Shiozawa, H. *et al.* Spontaneous emergence of long-range shape symmetry. *Nano Lett.* **11**, 160–163 (2011).
15. Egolf, D., Melnikov, I. & Bodenschatz, E. Importance of local pattern properties in spiral defect chaos. *Phys. Rev. Lett.* **80**, 3228–3231 (1998).
16. Egolf, D., Melnikov, I., Pesch, W. & Ecke, R. Mechanisms of extensive spatiotemporal chaos in Rayleigh-Bernard convection. *Nature* **404**, 733–736 (2000).
17. Warner, J. H. *et al.* Dislocation-driven deformations in graphene. *Science* **337**, 209–212 (2012).
18. Qian, L. *et al.* Control of the morphology and composition of yttrium fluoride via a salt-assisted hydrothermal method. *Crystengcomm* **12**, 199–206 (2010).
19. Tian, N., Zhou, Z.-Y., Sun, S.-G., Ding, Y. & Wang, Z. L. Synthesis of tetrahedral platinum nanocrystals with high-index facets and high electro-oxidation activity. *Science* **316**, 732–735 (2007).
20. Xia, Y., Xiong, Y., Lim, B. & Skrabalak, S. E. Shape-Controlled Synthesis of Metal Nanocrystals: Simple Chemistry Meets Complex Physics? *Angewandte Chemie International Edition* **48**, 60–103 (2009).
21. Maksimuk, S., Teng, X. & Yang, H. Roles of twin defects in the formation of platinum multipod nanocrystals. *Journal of Physical Chemistry C* **111**, 14312–14319 (2007).
22. Feng, J. & Zeng, H. C. Reduction and reconstruction of co₃o₄ nanocubes upon carbon deposition. *Journal of Physical Chemistry B* **109**, 17113–17119 (2005).
23. Baker, R. T. K., Harris, P. S. & Terry, S. Unique form of filamentous carbon. *Nature* **253**, 37–39 (1975).
24. Motojima, S., Ueno, S., Hattori, T. & Goto, K. Growth of regularly coiled spring-like fibers of si₃n₄ by iron impurity-activated chemical vapor-deposition. *Applied Physics Letters* **54**, 1001–1003 (1989).
25. Morin, A. S., Bierman, J. M., Tong, J. & Jin, S. Mechanism and kinetics of spontaneous nanotube growth driven by screw dislocation. *Nature* **328**, 476–480 (2010).
26. Ihara, S., Itoh, S. & Kitakami, J. Helically coiled cage forms of graphitic carbon. *Phys. Rev. B* **48**, 5643–5647 (1993).
27. Kawaguchi, M., Nozaki, K., Motojima, S. & Iwanaga, H. A growth-mechanism of regularly coiled carbon-fibers through acetylene pyrolysis. *Journal of Crystal Growth* **118**, 309–313 (1992).

Acknowledgements

H. S. and S. R. P. S. acknowledge the Leverhulme Trust for support through an early career fellowship. D. C. C. and S. R. P. S. thank the EPSRC and National Physical Laboratory for supporting the research. T. P. acknowledges support from the Austrian Science Funds (FWF Proj.Nr. I 943-N19). We thank J. Underwood, C. Buxey, D. Mansfield, T. Corless, M. Blissett and S. Loyer for technical assistance.

Author contributions

H.S. and S.R.P.S. conceived the ideas, and H.S. designed the experiments. H.S. and D.C.C. prepared the samples. H.S., A.B. and M.H.R. performed the experiments. H.S., A.B. and A.S. analysed the data. H.S., A.B., S.R.P.S., M.H.R. and T.P. wrote and reviewed the manuscript.

Additional information

Supplementary information accompanies this paper at <http://www.nature.com/scientificreports>

Competing financial interests: The authors declare no competing financial interests.

License: This work is licensed under a Creative Commons Attribution-NonCommercial-ShareAlike 3.0 Unported License. To view a copy of this license, visit <http://creativecommons.org/licenses/by-nc-sa/3.0/>

How to cite this article: Shiozawa, H. *et al.* Microscopic insight into the bilateral formation of carbon spirals from a symmetric iron core. *Sci. Rep.* **3**, 1840; DOI:10.1038/srep01840 (2013).